

Supplementary Material to Big Bang Nucleosynthesis Limits and Relic Gravitational Waves Detection Prospects

Tina Kahniashvili,^{1,2,3,*} Emma Clarke,^{1,†} Jonathan Stepp,^{1,‡} and Axel Brandenburg^{4,5,2,1,§}

¹*McWilliams Center for Cosmology and Department of Physics,
Carnegie Mellon University, Pittsburgh, PA 15213, USA*

²*School of Natural Sciences and Medicine, Ilia State University, 0194 Tbilisi, Georgia*

³*Abastumani Astrophysical Observatory, Tbilisi, GE-0179, Georgia*

⁴*Nordita, KTH Royal Institute of Technology and Stockholm University, 10691 Stockholm, Sweden*

⁵*Department of Astronomy, AlbaNova University Center, Stockholm University, 10691 Stockholm, Sweden*

(Dated: March 17, 2022)

I. MAGNETIC FIELD BOUNDS

The bound on extra relativistic degrees of freedom at big bang nucleosynthesis (BBN) can be expressed as

$$\frac{\rho_B(T_{\text{BBN}})}{\rho_\gamma(T_{\text{BBN}})} = f, \quad (1)$$

where we have assumed that all the extra relativistic energy density is entirely due to the magnetic energy density ρ_B , ρ_γ is the energy density in photons, T_{BBN} is the temperature of helium synthesis and $f \equiv \frac{7}{8} \left(\frac{4}{11}\right)^{4/3} \Delta N_{\text{eff}}$.

The photon energy density as a function of temperature is $\rho_\gamma = (\pi^2/15) T_\gamma^4$. The magnetic energy density is related to the magnetic field strength B as $\rho_B = B^2/8\pi$ (in Gaussian units). The magnetic field strength dilutes with the expansion of the universe as $B \sim a^{-2}$ where a is the cosmological scale factor. The comoving magnetic field strength is given by $B^{\text{co}} = (a/a_0)^2 B(a)$, where a_0 is the scale factor today. Substituting these values into the equation 1, the BBN limit on the field strength today is given by

$$B_*^{\text{co}} \leq \left(\frac{a_{\text{BBN}}}{a_0}\right)^2 \sqrt{8\pi f \rho_\gamma(T_{\text{BBN}})}. \quad (2)$$

Obtaining the ratio of the scale factors via entropy conservation, normalizing such that $a_0 = 1$, the bound is given by

$$\frac{B_*^{\text{co}}}{\text{Gauss}} \leq (8.06 \times 10^{-6}) f^{1/2} g_{\text{BBN}}^{-2/3} \quad (3)$$

where g_{BBN} is the relativistic degrees of freedom at T_{BBN} . There is no explicit dependence on temperature, however, the total number of relativistic degrees of freedom g_{BBN} does depend on the temperature. At $T_{\text{BBN}} = 0.1$ MeV, the temperature at which deuterium synthesis starts, neutrinos have already decoupled, electrons

and positrons have already become nonrelativistic, and $g_{\text{BBN}}(T = 0.1\text{MeV}) \simeq 3.4$. For $\Delta N_{\text{eff}} = 0.122$, we find $f = 0.028$ and the maximum comoving field strength at BBN is $B_{\text{BBN}}^{\text{max}} = 6.2 \times 10^{-7}$ G.

II. NUMERICAL SET-UP/GRAVITATIONAL WAVES

We consider the radiation-dominated epoch at electroweak (EW) and quantum chromodynamic (QCD) energy scales and compute the strains h_+ and h_\times for the two linear polarization modes by solving the linearized equation for gravitational waves (GWs),

$$\frac{\partial^2}{\partial t^2} \tilde{h}_{+/\times} + \mathbf{k}^2 \tilde{h}_{+/\times} = \frac{6}{a} \tilde{T}_{+/\times}, \quad (4)$$

where $\tilde{T}_{+/\times}$ are the + and \times polarizations of the Fourier transform of the total stress $\mathbb{T}_{ij} = u_i u_j - B_i B_j$, normalized by the radiation energy density, with t and \mathbf{k} the time and wave vector normalized by the Hubble parameter at the time of generation, and $\mathbf{B} = \nabla \times \mathbf{A}$ and \mathbf{u} are obtained by solving the equation for the magnetic vector potential

$$\frac{\partial \mathbf{A}}{\partial t} = \mathbf{u} \times \mathbf{B} + \eta \nabla^2 \mathbf{A}, \quad (5)$$

together with [1]

$$\frac{\partial \mathbf{u}}{\partial t} = -\mathbf{u} \cdot \nabla \mathbf{u} - \frac{1}{4} \nabla \ln \rho + \frac{3}{4\rho} \mathbf{J} \times \mathbf{B} + \mathcal{F}_\nu + \mathcal{F}, \quad (6)$$

$$\frac{\partial \ln \rho}{\partial t} = -\frac{4}{3} (\nabla \cdot \mathbf{u} + \mathbf{u} \cdot \nabla \ln \rho) + \mathcal{H}, \quad (7)$$

where $\mathcal{F} = (\nabla \cdot \mathbf{u} + \mathbf{u} \cdot \nabla \ln \rho) \mathbf{u}/3 - [\mathbf{u} \cdot (\mathbf{J} \times \mathbf{B}) + \mathbf{J}^2/\sigma] \mathbf{u}/\rho$, and $\mathcal{H} = [\mathbf{u} \cdot (\mathbf{J} \times \mathbf{B}) + \mathbf{J}^2/\sigma]/\rho$ are higher order terms in the Lorentz factor that are retained in the calculation, and $\mathcal{F}_\nu = 2\nabla \cdot (\rho \nu \mathbf{S})/\rho$ is the viscous force, where $S_{ij} = \frac{1}{2}(u_{i,j} + u_{j,i}) - \frac{1}{3}\delta_{ij} \nabla \cdot \mathbf{u}$ are the components of the rate-of-strain tensor with commas denoting partial derivatives, and ν is the kinematic viscosity. In all cases considered below, we assume a magnetic Prandtl number of unity, i.e., $\nu/\eta = 1$. In Table I, we summarize

*Electronic address: tinatin@andrew.cmu.edu

†Electronic address: emmaclar@andrew.cmu.edu

‡Electronic address: jdstepp@andrew.cmu.edu

§Electronic address: brandenb@nordita.org

the parameters for runs a–d and A–D for the QCD and EW energy scales, respectively. Here, $h_{\text{rms}}^{\text{sat}}$ refers to the value of $\langle h_+^2 + h_\times^2 \rangle^{1/2}$ evaluated during the final stationary regime.

As in Ref. [2], hereafter K+21, we compute GW generation from magnetically driven turbulence. The driving is applied during the time interval $1 \leq t \leq 2$, where t is the conformal time. As in K+21, we then decrease the driving linearly in time until $t = 3$, when the driving is turned off completely. We perform series of runs where we vary the strength of the forcing f_0 and keep the viscosity ν unchanged. However, it is not possible to explore the regime of strong magnetic energy at the same small values of ν that we were able to use for smaller magnetic energies. This is because for strong magnetic fields, the turbulence becomes more intense and more viscosity is needed to dissipate all this energy at the finite numerical resolution available.

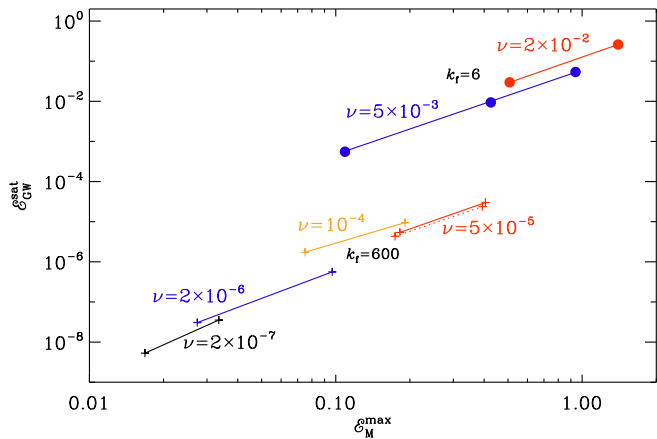


FIG. 1: Dependence of $\mathcal{E}_{\text{GW}}^{\text{sat}}$ on $\mathcal{E}_{\text{M}}^{\text{max}}$ for magnetically driven turbulence at different forcing strengths and viscosities for $k_f = 6$ (upper red and blue lines) and $k_f = 600$ (lower red, orange, blue, and black lines). The red dashed line for $k_f = 600$ denotes runs where the driving is turned off abruptly at $t = 2$.

In Fig. 1, we show the resulting dependence of the GW energy \mathcal{E}_{GW} on the magnetic energy \mathcal{E}_{M} for six sets of runs with fixed viscosity, different forcing strengths, and different forcing wavenumbers, corresponding to the runs denoted with labels a–d, A–D, and O. In all cases, we take the magnetic Prandtl number to be unity, i.e., the magnetic diffusivity is set equal to the value of ν . We also compare with several other sets of runs where we change the forcing.

In Table I, we summarize the parameters for four runs (A–D), which correspond to the less viscous ones for each of the four pairs shown in Fig. 1. One exception is Run D, which has the same viscosity as Run C and is denoted in Fig. 1 by a red line. Run D is the same one as Run M1 of K+21. The values of \mathcal{E}_{M} and \mathcal{E}_{GW} agree with those of K+21 for this run, but those of h_{rms} are here a bit

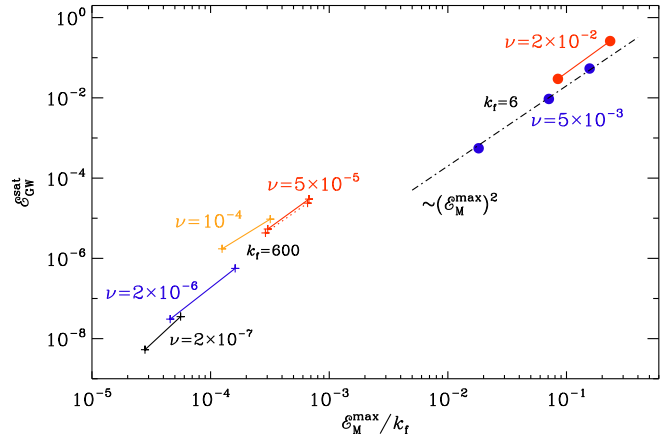


FIG. 2: Dependence of $\mathcal{E}_{\text{GW}}^{\text{sat}}$ on $\mathcal{E}_{\text{M}}^{\text{max}}/k_f$ for the same runs as in Fig. 1.

smaller. In fact, a closer inspection of the time series of $h_{\text{rms}}(t)$ revealed that it reaches a steady state much later than $\mathcal{E}_{\text{GW}}(t)$. Therefore, averaging can begin only later than for \mathcal{E}_{GW} . Since h_{rms} is found to decrease somewhat after having reached a maximum, the new value in Table I is now about 20% smaller than that given in K+21.

The data for \mathcal{E}_{GW} follow a power law scaling, $\propto \mathcal{E}_{\text{M}}^n$, where $n = 2.7$ for the points with the smallest viscosity. This is steeper than the quadratic scaling found in the work of [3], where the driving was applied for a much shorter time interval, $1 \leq t \leq 1.1$. Furthermore, for fixed values of ν , we find smaller local values of n , at least for the larger magnetic energies shown in Fig. 1. We also checked that these scalings are not significantly affected if the driving was turned off abruptly after $t = 2$. This is shown as the dotted line in Fig. 1 for $\nu = 5 \times 10^{-5}$.

Comparing the lines for $\nu = 5 \times 10^{-5}$ and $\nu = 10^{-4}$ in Figs. 1 and 2, we see that the decline of \mathcal{E}_{M} is stronger than that of \mathcal{E}_{GW} . This suggests that \mathcal{E}_{M} suffers more strongly from the increase of viscosity and magnetic diffusivity, and that \mathcal{E}_{GW} is less sensitive to the change of ν . However, one has to remember that GWs are solely the result of the magnetic and hydrodynamic stresses. One sees that the runs with smaller values of ν all have a faster rise of $\mathcal{E}_{\text{M}}(t)$ early on, which also translates into a rapid increase of $\mathcal{E}_{\text{GW}}(t)$. It is unclear, however, whether this aspect of the model with applied magnetic driving is realistic and whether this would also be borne out by a more physical implementation of a magnetogenesis model.

Next, we show in Fig. 3 the evolution of $\mathcal{E}_{\text{M}}(t)$ and $\mathcal{E}_{\text{GW}}(t)$ with time. We see that for Runs C and D, \mathcal{E}_{M} has reached a plateau well before $t = 2$, while for Run A, a maximum is reached only at $t = 2$, i.e., the time when the driving is decreased. Moreover, for Run A, there is a strong temporal decline of magnetic energy due to strong viscous damping. Nevertheless, similar GW energies are obtained in this case. The value of $\mathcal{E}_{\text{GW}} = 3 \times 10^{-5}$ given in Table I corresponds to $h_0^2 \Omega_{\text{GW}} = 4.93 \times 10^{-10}$, which

TABLE I: Summary of the runs.

Run	f_0	ν	\mathcal{E}_M^{\max}	$\mathcal{E}_{\text{GW}}^{\text{sat}}$	$h_{\text{rms}}^{\text{sat}}$	$B_{\text{rms}} [\mu\text{G}]$	$h_0^2 \Omega_{\text{GW}}$	h_c
Fa	5×10^{-1}	2×10^{-2}	1.40×10^{-0}	2.6×10^{-1}	2.7×10^{-1}	4.7	8.04×10^{-6}	2.69×10^{-13}
a2	3×10^{-1}	2×10^{-2}	5.08×10^{-1}	3.0×10^{-2}	9.2×10^{-2}	2.9	9.19×10^{-7}	9.19×10^{-14}
b	3×10^{-1}	5×10^{-3}	9.40×10^{-1}	5.4×10^{-2}	1.4×10^{-1}	3.9	1.66×10^{-6}	1.36×10^{-13}
c	2×10^{-1}	5×10^{-3}	4.26×10^{-1}	9.4×10^{-3}	5.7×10^{-2}	2.6	2.90×10^{-7}	5.73×10^{-14}
d	1×10^{-1}	5×10^{-3}	1.09×10^{-1}	5.5×10^{-4}	1.4×10^{-2}	1.3	1.71×10^{-8}	1.38×10^{-14}
A	7×10^{-3}	5×10^{-5}	4.05×10^{-1}	3.0×10^{-5}	3.1×10^{-5}	2.5	4.93×10^{-10}	2.46×10^{-20}
A'	7×10^{-3}	5×10^{-5}	3.94×10^{-1}	2.4×10^{-5}	2.7×10^{-5}	2.5	3.91×10^{-10}	2.19×10^{-20}
A2	7×10^{-3}	1×10^{-4}	1.91×10^{-1}	9.5×10^{-6}	2.0×10^{-5}	1.8	1.56×10^{-10}	1.61×10^{-20}
O1	5×10^{-3}	5×10^{-5}	1.82×10^{-1}	5.4×10^{-6}	1.4×10^{-5}	1.7	8.86×10^{-11}	1.12×10^{-20}
O1'	5×10^{-3}	5×10^{-5}	1.74×10^{-1}	4.3×10^{-6}	1.2×10^{-5}	1.7	7.07×10^{-11}	9.65×10^{-21}
O2	5×10^{-3}	1×10^{-4}	7.50×10^{-2}	1.7×10^{-6}	8.4×10^{-6}	1.1	2.84×10^{-11}	6.67×10^{-21}
B	2×10^{-3}	2×10^{-6}	9.67×10^{-2}	5.6×10^{-7}	5.2×10^{-6}	1.2	9.24×10^{-12}	4.17×10^{-21}
C2	1×10^{-3}	2×10^{-6}	2.74×10^{-2}	3.1×10^{-8}	1.3×10^{-6}	0.66	5.03×10^{-13}	1.03×10^{-21}
C	1×10^{-3}	2×10^{-7}	3.35×10^{-2}	3.5×10^{-8}	1.3×10^{-6}	0.73	5.80×10^{-13}	1.07×10^{-21}
D	6×10^{-4}	2×10^{-7}	1.68×10^{-2}	5.3×10^{-9}	7.1×10^{-7}	0.52	8.73×10^{-14}	5.64×10^{-22}

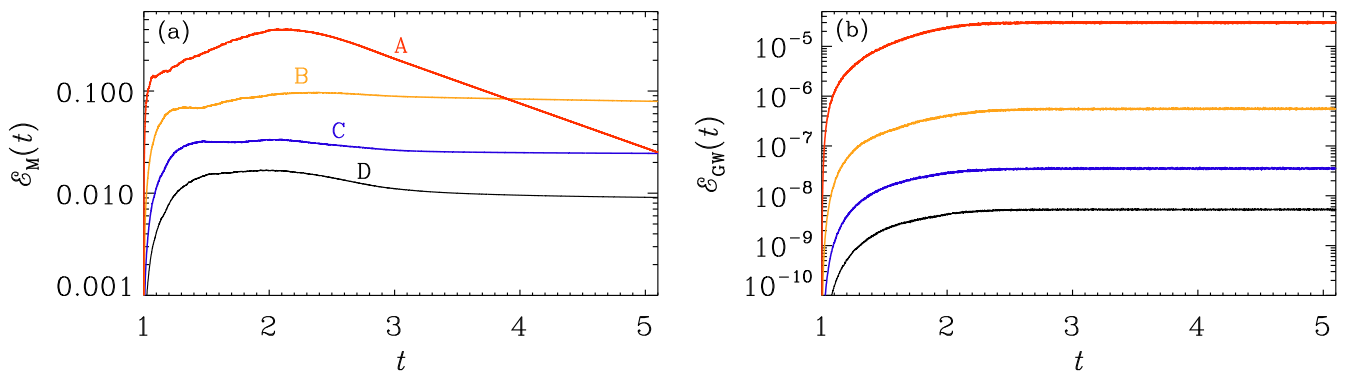


FIG. 3: Evolution of (a) $\mathcal{E}_M(t)$ and (b) $\mathcal{E}_{\text{GW}}(t)$ for Runs A–D of Table I. Note the rapid decay for Run A with the largest viscosity.

is four orders of magnitude larger than for Run D.

-
- [1] A. Brandenburg, K. Enqvist, and P. Olesen, Phys. Rev. D **54**, 1291 (1996), astro-ph/9602031.
[2] T. Kahniashvili, A. Brandenburg, G. Gogoberidze, S. Mandal, and A. Roper Pol, Phys. Rev. Res. **3**, 013193 (2021), 2011.05556.

- [3] A. Roper Pol, S. Mandal, A. Brandenburg, T. Kahniashvili, and A. Kosowsky, Phys. Rev. D **102**, 083512 (2020), 1903.08585.